Ultrasound in Med. & Biol., Vol. 45, No. 8, pp. 2104–2117, 2019

0301-5629/$ - see front matter

https://doi.org/10.1016/j.ultrasmedbio.2019.04.010

● *Original Contribution*

INTRACRANIAL NON-THERMAL ABLATION MEDIATED BY TRANSCRANIAL FOCUSED ULTRASOUND AND PHASE-SHIFT NANOEMULSIONS

CHENGUANG PENG,*,† TAO SUN,† NATALIA VYKHODTSEVA,† CHANIKARN POWER,† YONGZHI ZHANG,† NATHAN MCDANNOLD,† and TYRONE PORTER*

* Department of Biomedical Engineering, Boston University, Boston, Massachusetts, USA; and † Department of Radiology, Brigham and Women's Hospital, Boston, Massachusetts, USA

(*Received* 21 *August* 2018; *revised* 18 *March* 2019; *in final from* 7 *April* 2019)

Abstract—High intensity focused ultrasound (HIFU) mechanical ablation is an emerging technique for non-invasive transcranial surgery. Lesions are created by driving inertial cavitation in tissue, which requires significantly less peak pressure and time-averaged power compared with traditional thermal ablation. The utility of mechanical ablation could be extended to the brain provided the pressure threshold for inertial cavitation can be reduced. In this study, the utility of perfluorobutane (PFB)-based phase-shift nanoemulsions (PSNEs) for lowering the inertial cavitation threshold and enabling focal mechanical ablation in the brain was investigated. We successfully achieved vaporization of PFB-based PSNEs at 1.8 MPa with a 740 kHz focused transducer with a pulsed sonication protocol (duty cycle = 1.5%, 10 min sonication) within intact CD-1 mice brains. Evidence is provided showing that a single bolus injection of PSNEs could be used to initiate and sustain inertial cavitation in cerebrovasculature for at least 10 min. Histologic analysis of brain slices after HIFU exposure revealed ischemic and hemorrhagic lesions with dimensions that were comparable to the focal zone of the transducer. These results suggest that PFB-based PSNEs may be used to significantly reduce the inertial cavitation threshold in the cerebrovasculature and, when combined with transcranial focused ultrasound, enable focal intracranial mechanical ablation. (E-mail: pcg11@bu.edu)

Key Words: **Focused ultrasound, Brain, Non-thermal ablation, Phase-shift nanoemulsions, Microbubble, Ultrasound therapy.**

INTRODUCTION

High intensity focused ultrasound (HIFU) ablation has drawn increasing attention in recent years as an alternative to surgical resection of brain tumors. Surgical resection is part of the standard of care for brain tumors (Weller et al. 2014). Patients with brain tumors are usually recommended to undergo surgical resection if possible, and there is evidence that more aggressive resections significantly improve the overall survival rate (Chaichana et al. 2014a, 2014b). However, for many patients, surgical resection is not an option because of the proximity of the tumor to critical vascular and neural systems (De la Garza-Ramos et al. 2016). Moreover, surgical removal of a brain tumor is an invasive procedure that is challenging and risky to patients of advanced age and poor health (Karsy et al. 2018). Therefore, an alternative method to surgical resection that can non-invasively ablate brain tumors that are deemed inoperable is highly desired. To our knowledge, HIFU is the only completely non-invasive method available on the market that can access and locally ablate inoperable tumors.

HIFU technology utilizes a focused ultrasound (FUS) transducer to transmit ultrasonic waves non-invasively and ablate targeted tissue either thermally or mechanically (Coluccia et al. 2014). Currently, HIFU thermal ablation has been approved by the U.S. Food and Drug Administration for various clinical indications, including uterine fibroid ablation, palliation for bone metastases, prostate tissue ablation and essential tremors (Elias et al. 2016; Gianfelice et al. 2008; Koch et al. 2007; Stewart et al. 2006). HIFU thermal ablation utilizes the heat generated by the absorption of FUS to coagulate tissues. To enable brain applications, transcranial magnetic resonance imaging (MRI)-guided HIFU systems have been developed and shown to be capable

Address correspondence to: Chenguang Peng, 221 Longwood Avenue, Room 514, Boston, MA, USA, 02115. E-mail: pcg11@bu.edu

of thermally ablating brain tumors (Coluccia et al. 2014; McDannold et al. 2010).

There are several critical challenges for the application of HIFU thermal ablation in the brain. One of the critical issues is the utilization of high time-averaged power (*i.e.,* over 1000 W), which could result in skull heating when treating peripheral brain regions. Long periods between sonications are also required to allow for the skull to cool, prolonging the treatment and making it challenging to ablate more than tiny volumes (Coluccia et al. 2014). Furthermore, the incidence angle between the incident ultrasound and the skull is large when targeting peripheral regions (White et al. 2006). This significantly increases the reflection of the ultrasound so that the energy deposition efficiency is further reduced. The limitation was evident in an MRI temperature measurement of a patient with a tumor in which surface heating was observed (McDannold et al. 2010). Standing waves induced within the skull by the long ultrasound bursts typically utilized for thermal ablation is another issue to be considered. The results of experiments and numerical simulations have shown that long tone bursts can create standing wave patterns in the brain, leading to unwanted thermal coagulation outside the focus (Azuma et al. 2005; Baron et al. 2009; Junho Song et al. 2012; Wang et al. 2008). To overcome these problems, transcranial MRI-guided FUS systems using hemispherical phased arrays have been developed (Elias et al. 2016). These systems mitigate heating in the skull by delivering energy to the focus through a larger aperture and using active cooling (Elias et al. 2016; Huss et al. 2015; McDannold et al. 2010). Despite these technical advancements, targeting the surface of the brain remains a challenge. Therefore, there is a need for new ablation methods that use significantly lower time-averaged power for treating superficial regions.

One way to dramatically decrease the time-averaged acoustic power is to use mechanical ablation instead of thermal ablation. Mechanical ablation—including histotripsy (Khokhlova et al. 2015; Roberts et al. 2006) and microbubble (MB)-facilitated mechanical ablation (Arvanitis et al. 2016; Burke et al. 2011; McDannold et al. 2006)—has been explored over the last decade as an alternative to thermal ablation. Unlike thermal ablation, mechanical ablation typically uses short pulses, which limits the overall heat generation during the treatment. Histotripsy treatment uses short pulses at pressures exceeding the intrinsic cavitation threshold in tissue (Vlaisavljevich et al. 2015), creating bubble clouds at the focus that homogenize tissue in a highly localized manner (Xu et al. 2005). However, the pressure used in histotripsy—usually above 20 MPa (Khokhlova et al. 2014; Maxwell et al. 2011; Wang et al. 2013; Zhang et al. 2015)—is even higher than in thermal ablation, which could result in safety concerns. In contrast, MB-facilitated ablation takes advantage of pre-formed MBs (*i.e.* ultrasound contrast agents) that are injected into the bloodstream. The MBs are driven to oscillate with the ultrasound and generate stresses that can adversely affect blood vessels, resulting in a significant reduction in tumor perfusion leading to cancer cell death (Al-Mahrouki et al. 2014; Czarnota et al. 2012). The pressure magnitude required for this bioeffect is three orders of magnitude smaller than the thermal ablation (*i.e.,* 300 W vs. 0.1 W). Additionally, the duty cycle that determines the on/off ratio of the ultrasound transmission is two orders lower (*i.e.,* 1% vs. 100% for MB-facilitated vs. thermal ablation) (Huang et al. 2013; McDannold et al. 2006, 2013, 2016). MBs, when injected intravenously (IV), circulate in the bloodstream and cavitate in response to incident ultrasound waves, generating stresses that mechanically ablate tissues (McDannold et al. 2006). However, researchers have been concerned about the damage along the ultrasound pathway due to non-linear bubble oscillations in the pre-focal zones (Arvanitis et al. 2016; Moyer et al. 2015; Phillips et al. 2013). Furthermore, commercial MBs (*i.e.,* ultrasound contrast agents) usually circulate for only a few minutes (Wu et al. 2017), so a volumetric ablation of the tumor would require continuous infusion of MBs, which is dose limited.

Because of those limitations, using phase-shift nanoemulsions (PSNEs) to facilitate mechanical ablation has been proposed. PSNEs have a lipid monolayer shell with a liquid perfluorocarbon core (Kopechek et al. 2014; Sheeran et al. 2012). PSNEs can be vaporized into bubbles when they are exposed to ultrasound that has peak negative pressure (PNP) higher than the vaporization threshold (Fabiilli et al. 2010; Schad and Hynynen 2010; Zhang and Porter 2010). Therefore, it is possible to only activate PSNEs and create lesions at the focus while sparing tissue in the pre-focal zones. Submicron perfluorocarbon droplets have been synthesized with a mean diameter of approximately 200 nm and PEGylated lipid on the surface, which prolonged the circulation in the vasculature (Suk et al. 2016; Zhang et al. 2013). Nanoparticles at the range of 50−600 nm have a higher chance to accumulate in tumors because of the leaky vasculature and immature lymphatic drainage system, a phenomenon called the enhanced permeability (EPR) effect (Charrois and Allen 2003; Ishida et al. 1999; Maeda et al. 2000; Nomura et al. 1998; Yuan et al. 1995). By virtue of the EPR effect, PSNEs have a higher possibility than MBs to accumulate into tumors, making them potentially better candidates for mechanical tumor ablation.

Previously, our group injected perfluoropentane (PFP) PSNEs IV. and observed an accumulation of PFP PSNEs within the implanted tumor in a rabbit (Kopechek

et al. 2014). A lesion was created successfully in that study. However, the vaporization threshold of PFP PSNEs was 3−5 MPa, which potentially would cause severe adverse effects in the brain, particularly at the lower frequencies used for transcranial sonication. We were therefore encouraged to look for another formulation to synthesize PSNEs with a more volatile perfluorocarbon, such as perfluorobutane (PFB). PFB-based nanoemulsions produced using a MB condensation method (Sheeran et al. 2011, 2012) reportedly have been vaporized at pressures less than 2 MPa (Sheeran et al. 2013), which is a more ideal pressure for ultrasound applications in the brain.

In this study, we investigated ultrasound-induced vaporization of PFB-based PSNEs at 740 kHz, which is a clinically relevant frequency (*i.e.,* 650 kHz for Exablate Neuro system, INSIGHTEC Ltd, Tirat Carmel, Israel) for transcranial applications (Clement et al. 2000). There have only been limited investigations on the vaporization of PSNEs using a transducer operating below 1 MHz (Giesecke and Hynynen 2003; Schad and Hynynen 2010). The acoustic signatures of PSNEs at sub-MHz frequency range is thus vital for monitoring and control of PSNE vaporization in the brain. Our objectives here were to use PFB PSNEs to lower the mechanical ablation threshold in the brain through an intact skull in a mouse model. Broadband acoustic emissions recorded with a passive cavitation detector (PCD) were monitored during each sonication. The lesions were characterized through histologic analysis.

MATERIALS AND METHODS

Emulsion preparation

PSNEs were prepared using a cooling and condensation protocol described in Sheeran et al. (2012). In brief, the lipid solution was formed from 1,2-dipalmitoyl-sn-glycero-3-phosphocholine and 1,2-distearoyl-sn-glycero-3-phosphoethanolamine-N-[amino(polyethylene glycol)-2000] from Avanti Lipids (Alabaster, AL, USA) in a 95:5 molar ratio. Lipids (45 mg in total) were dissolved in chloroform for a thorough mixture. The solvent was evaporated, and the dry lipid film was rehydrated with 15 mL phosphate-buffered saline (PBS) at 60°C to achieve a final concentration of 3 mg/mL lipid solution. The lipid solution was sonicated for 2 min at 20% power (100 Watt at 20 kHz) using a Vibra-Cell probe sonicator (VC 505, Sonics & Materials, Newtown, CT, USA) at room temperature right before use. A 0.75 mL volume of lipid solution was transferred to a 1.5 mL glass vial with a septum cap. The cap space was then ventilated with 4 mL PFB gas. An additional 6 mL volume of PFB gas was injected into the vial. A high-speed shaker was then used to shake the vial for 30 s to generate MBs. The MB solution was transferred into a 7 mL glass vial with 5 mL PBS. The PBS was degassed overnight, and the cap space then was replaced with PFB gas. The glass vial was then put into an acetone dry ice bath, which was kept at −5°C to −10°C. The vial was pressurized with PFB until the solution became clear, which indicated a transition from MBs to nanoemulsions, followed by 3 passes through 200 nm polycarbonate membrane filters (Whatman, Piscatway, NJ, USA) using a LIPEX extruder (Northern Lipids, Burnaby, BC, Canada). The resulting PSNE solution was kept in the 7 mL glass vial with the headspace filled with PFB gas at 20 psi. The PSNE solution was stored in the refrigerator until use. The synthesized PSNEs were diluted and measured with qNano (Izon science, Cambridge, MA, USA). The mean PSNE diameter was 226 ± 7.3 nm, and the mean concentration was $5.2 \pm 1.4 \times 10^9$ particles/mL.

Animals

Experiments were performed in accordance with procedures approved by the Brigham and Women's Institutional Animal Care and Use Committee. Experiments were performed in 12 male CD-1 mice each weighing 25−30 g. Animals were anesthetized with ketamine and xylazine. The hair on the head was removed beforehand, a catheter was placed in the tail vein and PSNEs (100 μL) were administered as a bolus injection for all animals (N = 12).

FUS ablation

A focused circular transcranial ultrasound transducer was built in house with a 10 cm aperture and 8 cm curvatures. The center frequency of the transducer was 740 kHz. The transducer was driven by sinusoidal waves produced by a function generator (Agilent 33250 A, Santa Clara, CA, USA) and amplified by a power amplifier (ENI 2100 L, Bell Electronics, Renton, WA, USA). Electrical power output from the amplifier was measured using a power meter (E4419 B, Agilent, Santa Clara, CA, USA) and a dual directional coupler (model C5948, Werlatone, Patterson, NY, USA). A laboratory-assembled radiation force balance was used to measure the acoustic power transmitted from the transducer in degassed water. Additionally, the transmitted pressure field was mapped using a needle hydrophone (HNC-0200, Onda, CA, USA). As is shown in Figure 1b, the transverse and longitudinal full width at half maximum (FWHM) of the transducer focus were 2.5 and 11.7 mm, respectively.

As is shown in Figure 1a, the transducer was mounted on a manually adjustable three-axis translation stage and submerged into degassed deionized water within an acrylic tank. The animals were placed in a plastic stereotactic frame (constructed in house), which

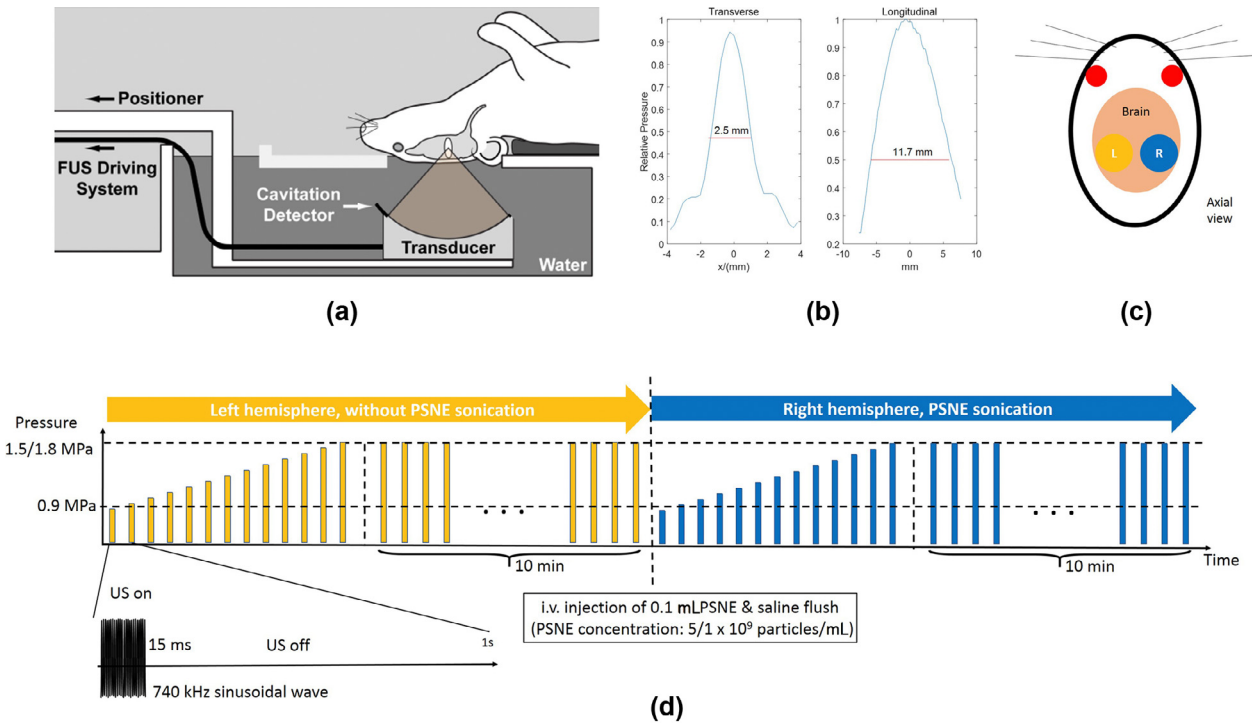

Fig. 1. (a) Experimental setup. A focused transducer and a cavitation detector were mounted on a manually adjustable 3-D positioner located in a water tank. The mice were held by a customized holder in a supine position. (b) The longitudinal and transverse pressure profiles of the focused transducer. (c) Schematic of the targets' location. (d) Timeline and schematic of sonication protocol. For each animal, the left hemisphere was sonicated first, and then 0.1 mL PSNEs in different concentrations was administered before the right hemisphere was sonicated. For each sonication on both hemispheres, a series of ramping pressure pulses were applied, followed by 10 min constant pressure pulses. Each pulse consisted of a 15 ms 740 kHz sinusoidal wave repeated at 1 Hz. FUS = focused ultrasound; IV = intravenous; PSNE = phase-shift nanoemulsions; US = ultrasound.

was attached so that the animals were supine with the top of their head in the water bath. The targets were selected from a mouse brain atlas (Paxinos and Franklin 2004) and were centered 2.5 mm lateral, 3 mm dorsal and 3 mm anterior. As is shown in Figure 1c, each animal has two sonications located at a region 1.5 mm above the hippocampus on both hemispheres (left hemisphere: sonication without PSNEs started from 0 min; right hemisphere: after sonication of left hemisphere and IV injection of PSNEs followed by saline flush). Sonication protocol is described in Figure 1d. Each sonication started with a series of 15 ms pulses repeated at 1 Hz, and each pulse had the pressure increased from 0.9 MPa to 1.5/1.8 MPa at 0.18 MPa pressure interval (four mice with 1.8 MPa and four mice with 1.5 MPa). Immediately after that, constant pressure (the maximum pressure used in ramping pressure pulses) pulses with 15-ms burst lengths that repeated at 1 Hz were used to sonicate the brain for 10 min (four mice with 1.8 MPa and four mice with 1.5 MPa). The corresponding time-averaged acoustic power for 1.5 MPa and 1.8 MPa was approximately 0.17 and 0.24 W, respectively. To understand the effect of PSNE concentration on the ablation, another group of animals (four mice) were sonicated with 1.8 MPa after injection of diluted PSNEs (dilution factor = five). The five times dilution factor was chosen based on a pilot study from our group (unpublished) that showed no apparent damage was generated at this condition. All other acoustic parameters remained the same. The summary of the acoustic parameters and PSNE concentrations for the different groups is shown in Table 1.

Table 1. List of key parameters for different groups

Group	Pressure (MPa)	PSNE concentration (particles/mL)	Number of mice
High pressure high PSNE concentration	1.8	$5.2 \pm 1.4 \times 10^9$	4
Low pressure high PSNE concentration	1.5	$5.2 \pm 1.4 \times 10^9$	4
High pressure low PSNE concentration	1.8	$1.0 \pm 0.3 \times 10^9$	4

PSNE = phase-shift nanoemulsions.

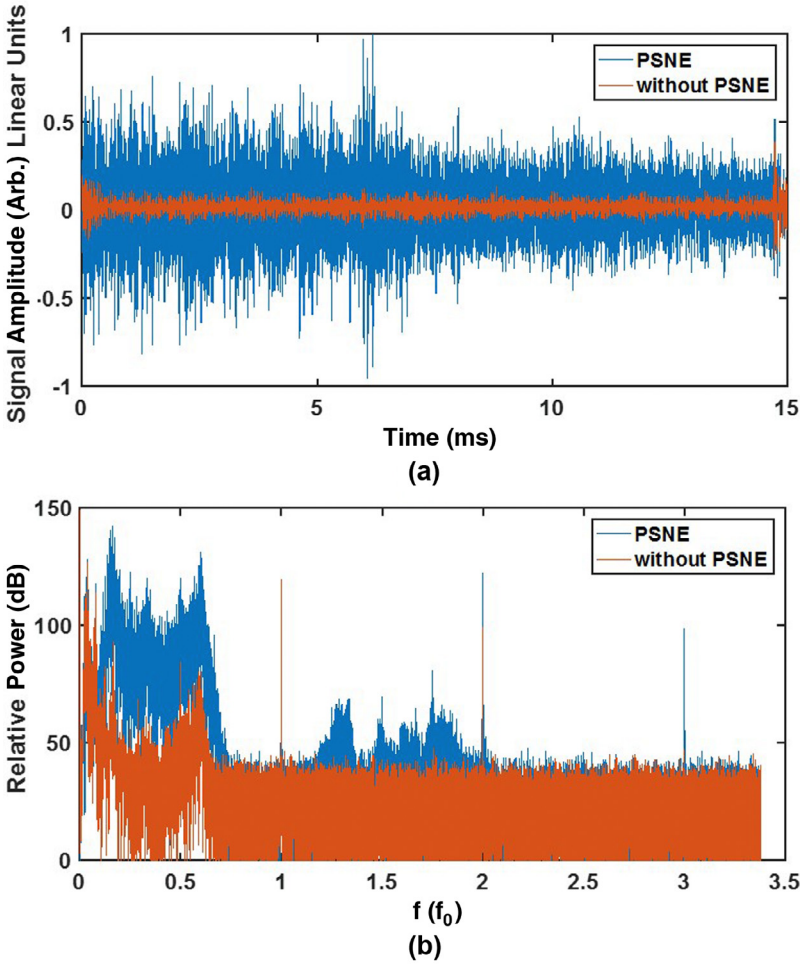

Fig. 2. (a) time domain signal of acoustic emissions obtained during 1.8 MPa bursts applied with and without PSNEs. The sonication started at 0 ms and ended at 15 ms. (b) the corresponding frequency domain power spectrum as a function of normalized frequency (f_0 = 740 kHz) for these two bursts. A significant elevation of signal at both temporal and frequency domain could be observed, indicating vaporization of PSNEs. Arb. = arbitrary; PSNE = phase-shift nanoemulsions.

Monitoring PSNE-nucleated inertial cavitation

Acoustic vaporization of PSNEs and subsequent inertial cavitation (IC) activity were monitored using a PCD. An unfocused 400-kHz transducer served as the PCD and was positioned orthogonally to and confocally with the FUS transducer. The PCD-acquired acoustic energy radiated at frequencies below 740 kHz, which could only be generated by non-linearly oscillating and collapsing MBs. Two notch filters (Customized Notch filter, FD: 660 kHz, Allen Avionics, Mineola, NY, USA; in-house notch filter with 740 kHz center frequency) were used to filter out the fundamental frequency from the transducer, and a digital pulse receiver (Pulser/Receiver 5072 PR, GE Panametrics, Waltham, MA, USA) was used as the amplifier for the PCD signal, providing 40 dB gain and operating in low-pass mode (cut off frequency 10 MHz). Acoustic emissions were digitized by a high-speed AD converter (PXIe 1073, National Instruments Corporation, Austin, TX, USA) at a sampling rate of 5 MHz.

Analysis of PSNE-nucleated IC

The PCD signals were processed and analyzed to determine a threshold for PSNE-nucleated IC and to characterize the IC activity. The IC threshold was determined by comparing the mean broadband acoustic emission power spectra (MBEPS) for the PSNE and no PSNE groups. The MBEPS was calculated as in eqn (1):

$$\mathrm{MBEPS}_i = \frac{20}{f_b}\, log_{10}\left(\int_{f_0-0.5f_b}^{f_0+0.5f_b} \frac{\mathrm{PS}_i(f)}{\mathrm{PS}_{noise}(f)}\, df\right),\ i = PSNE,\ NO\ PSNE \quad (1)$$

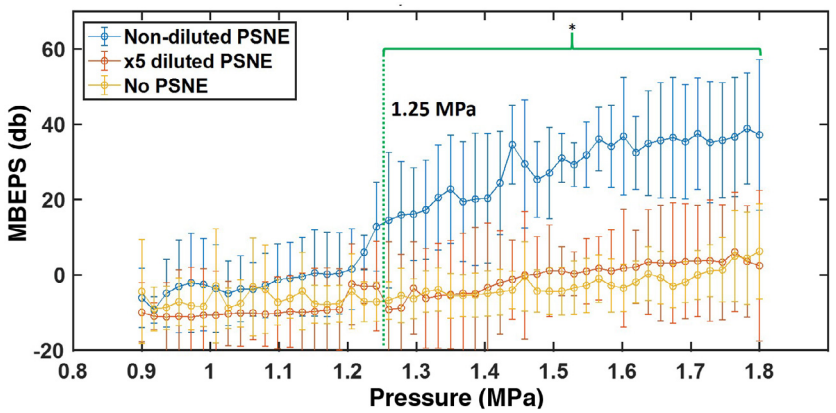

Fig. 3. Mean of broadband emission power spectra (MBEPS) from sonication with and without PSNEs as a function of the pressure amplitude. The green bracket indicates the pressure range that MBEPS of non-diluted PSNEs ($5.2 \pm 1.4 \times 10^9$ particles/mL) was significantly higher than for sonication without PSNEs. After 1.25 MPa, sonications with non-diluted PSNEs created significant higher MBEPS—a measurement of acoustic emission—than the sonication without PSNEs. MBEPS of × 5 diluted PSNEs ($1.0 \pm 0.3 \times 10^9$ particles/mL) has no significant difference with that obtained without PSNEs control, indicating a lack of PSNE-nucleated IC. (Mean ± standard deviation shown, N = 4 for the two PSNE groups. N = 8 for controls; $*p < 0.05$). IC = inertial cavitation; MBEPS = mean of broadband emission power spectra; PSNE = phase-shift nanoemulsions.

PS stands for power spectrum, which was the square of the signal spectrum calculated by a fast Fourier transform in MATLAB (MathWorks, Inc., Natick, MA, USA). f_0 represents the center frequency of the spectrum of interest, which was 370 kHz (subharmonic) in this study. f_b denotes the frequency bandwidth of the spectrum of interests, which was 40 kHz in this study. $PS_{noise}(f)$ was considered the power spectrum of the electronic noise of the system, which was estimated by averaging from five acquisitions without ultrasound transmission. The IC threshold was identified as the lowest pressure at which the $MBEPS_{PSNE}$ was statistically larger than $MBEPS_{NOPSNE}$. Two-sample Student's *t*-test with unequal variance was used for statistical analysis. The threshold for statistical significance was $p < 0.05$.

We speculated that IC activity, and thus the power within PCD signals, would vary with the concentration of administered PSNEs. To test the hypothesis, the enhancement in the PS for a PSNE group relative to a control group (*i.e.* no PSNE) was calculated and compared for the different administered concentrations of PSNEs. The relative enhancement in the PS within a given bandwidth was calculated as in eqn (2):

$$\text{Enhancement} = \frac{20}{f_b} \log_{10}\left(\int_{f_0-0.5f_b}^{f_0+0.5f_b} \frac{PS_{PSNE}(f)}{PS_{NOPSNE}(f)} df\right) \quad (2)$$

Histologic analysis

Animals were sacrificed within 24 h after treatment under deep anesthesia with isoflurane. The brains were fixed by cardiac perfusion using 0.9% NaCl (10 mL), followed by 10% buffered formalin phosphate (10 mL). The brains were then harvested and kept in 10% buffered formalin phosphate for at least 24 h before histology. Mice brains were then cut into two 3 mm blocks. Blocks were cut into 2 μm thickness sections, and every 50 sections were stained with hematoxylin and eosin (H&E). The lesions were manually selected by one investigator (C.P.) and analyzed with ImageJ (U. S. National Institutes of Health, Bethesda, Maryland, USA) to measure the lesion sizes. The areas of lesions from the group using non-diluted PSNEs sonicated with 1.8 MPa (the only group that had lesion at targeted area) were averaged (N = 4) and compared to the circular area of the transverse FWHM of the transducer acoustic focus.

RESULTS

PSNE vaporization and IC

Acoustic emissions received by the PCD were processed and compared across a range of conditions. Typical temporal and spectral signals from the PCD with and without PSNEs at 1.8 MPa are plotted in Figure 2. There was a significant increase in the peak voltage and the relative power of the PCD signal associated with PSNE vaporization and IC in the brain. Given that the bandwidth of the PCD was less than the frequency of the transmitted tone burst, the detected acoustic emissions should have originated only from cavitating MBs created in the acoustic field. Therefore, the representative traces in Figure 2 suggest that enough acoustic energy was transmitted through the skull to vaporize the PSNEs and drive IC activity.

The detected IC activity was quantified as MBEPS and plotted as a function of transmitted pressure (Fig. 3).

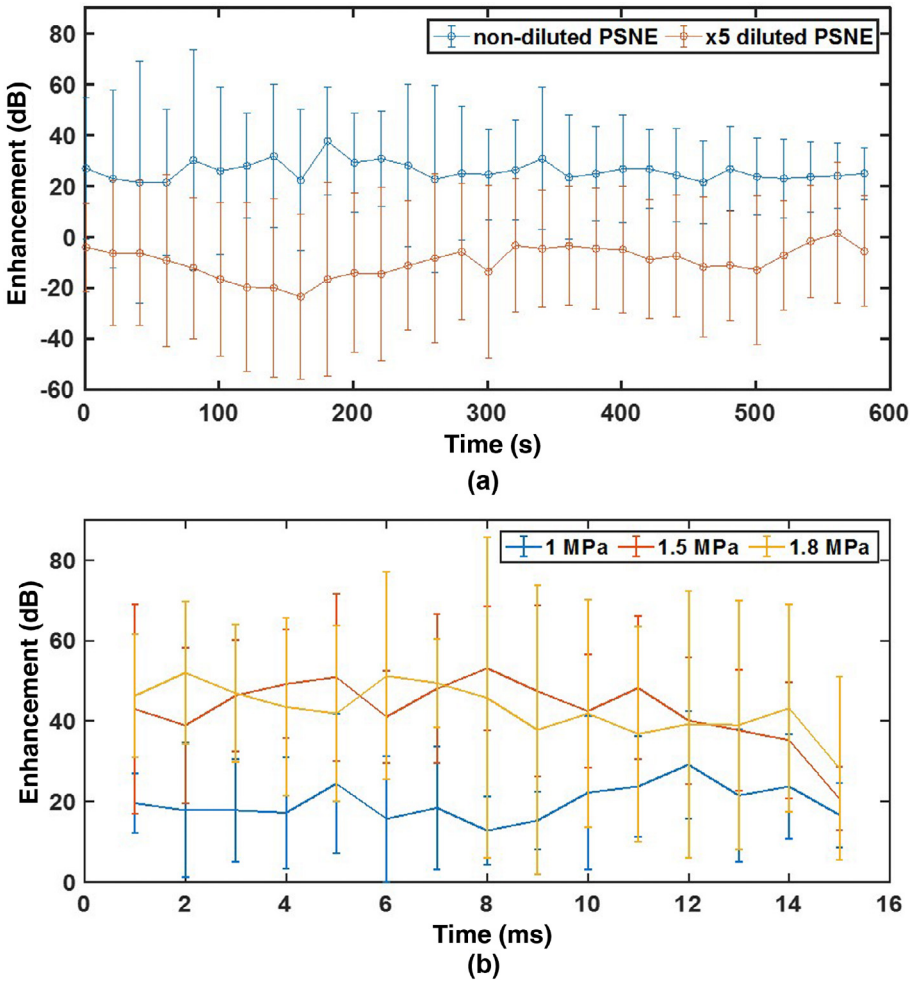

Fig. 4. (a) Acoustic emission enhancement of non-diluted and × 5 diluted PSNEs over 10 min. The enhancement stayed stable during 10 min, which indicated a constant activation of PSNEs during the whole sonication. (b) Acoustic emission enhancement as a function of time within each 15 ms burst during sonication at 1, 1.5 and 1.8 MPa. The acoustic emission enhancement is stable throughout the pulse length, indicating the PSNEs were vaporized as soon as the sonication started and that there were presumably enough PSNEs to be vaporized during the pulse. (N = 4 per group). PSNE = phase-shift nanoemulsions.

For the PSNE group ($5.2 \pm 1.4 \times 10^8$ injected particles), MBEPS did not change significantly until the pressure exceeded 1.2 MPa. The lowest non-derated pressure at which MBEPS for the PSNE group was significantly greater than MBEPS for the control group was 1.25 MPa ($p < 0.05$), which was identified as the IC threshold. Comparatively, there was no significant elevation of MBEPS generated from five times diluted PSNEs ($1.0 \pm 0.3 \times 10^8$ injected particles).

To further investigate PSNE vaporization and IC activity over a relatively longer period, 10-min sonications were applied after the ramping pulse and the acoustic emission enhancement was calculated and plotted in Figure 4a. Elevated acoustic emissions were detected throughout the 10-min exposure, indicating a continuous existence and vaporization of PSNEs in the bloodstream. The average enhancement acoustic emission within each 15-ms tone burst at 1 MPa, 1.5 MPa and 1.8 MPa is presented in Figure 4b. The results show that IC occurred over the entire duration of the tone burst, most likely sustained by PSNE vaporization.

Histologic analysis of PSNE-enhanced lesions

High pressure (1.8 MPa) and non-diluted PSNEs. Examinations of the lesions in tissue blocks showed hemorrhagic and ischemic lesions in the targeted area (right of Fig. 5a, 5b), and there was no apparent damage in the contralateral side (left side in Fig. 5a, 5c). Histologic examinations revealed that intense PSNE-nucleated IC activity at this pressure led to blood vessel rupture localized to the lesion (Fig. 6a, 6b).

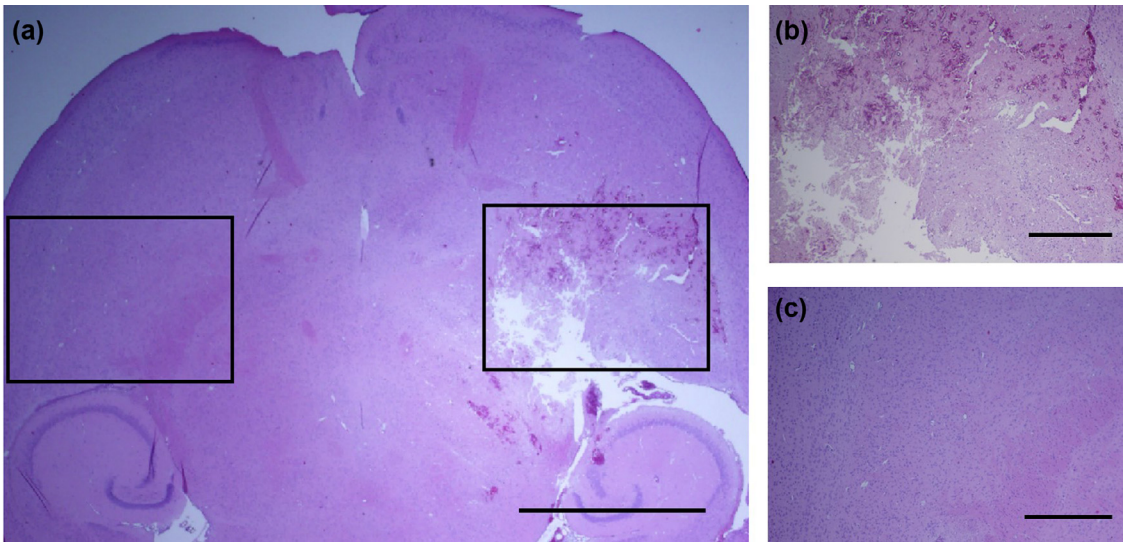

Fig. 5. Representative histologic slices from the mice that were injected with non-diluted PSNEs and were exposed to high ultrasound pressure. Lesions (1.5−2.5 mm in transverse dimension) were observed 24 h after the sonications in 4/4 mice. Hemorrhagic and ischemic lesions were formed at the targeted area. On the right side where they were sonicated without PSNEs, no apparent damage was observed. Scale bars are 2 mm in (a) and 0.5 mm in (b) and (c). PSNE = phase-shift nanoemulsions.

Erythrocyte extravasation was more obvious around large blood vessels, which could be due to the relatively lower IC threshold in larger blood vessels (Hynynen 1991). Damage to the microvasculature could disrupt the local blood supply, resulting in ischemic necrosis in the targeted area, as shown in Figure 6c. Tissue fragmentation could also be observed in Figure 6d, which was possibly the result of mechanical fragmentation.

Another example of the lesions from this group is presented in Figure 7. The lesion had a sharp boundary with a small transition area about 0.1−0.2 mm wide (Fig. 7b). The average area of lesion was 6.94 ± 1.26 mm^2, which was comparable with the 0.9 MPa transverse contour of the transducer (half of the peak pressure) as is shown in Figure 1b (diameter approximately 2.5 mm). It can be seen in Figure 7 that despite the substantial volume of this lesion in the mouse brain (approximately 10 mm), the hippocampus remained undamaged. Dead neurons with shrunken nuclei and without cytoplasm were also observed throughout the lesion, and pyknotic nuclei could be seen around the boundary of the lesion (Fig. 7b).

In some mice, PSNE-enhanced sonications created an empty cavity where proteinaceous fluid filled in and appeared in pink color. This was presumably due to the mechanical destruction of tissues, which created space for fluid to accumulate (Fig. 8a, 8b). Damage at the tissue boundary away from the target was seen in some mice between the white matter and gray matter and at meninges (Fig. 8c, 8d).

Low pressure (1.5 MPa) and non-diluted PSNEs. Four mice were sonicated with lower pressure (1.5 MPa) and non-diluted PSNEs. The pressure used in this group was still higher than the IC threshold determined from the acoustic measurements. In this group, three out of four mice had no apparent damage, as is shown in Figure 9 (c, d). One subject had hemorrhagic damage close to the base of the brain (Figure 9b). However, there was no apparent damage in the slice from the middle of the brain (Figure 9a). Considering the ultrasound propagation direction, which was from top to bottom of the skull, this was likely caused by the reflection from the skull, which increased the pressure close to the base of the brain and created unpredictable damage. Also, the resulted lesion was less than 1 mm in diameter, which was smaller than the lesion created for the 1.8 MPa exposures.

High pressure (1.8 MPa) and five times diluted PSNEs. Four mice were sonicated with high pressure (1.8 MPa) after administration of five times diluted PSNEs ($1.0 \pm 0.3 \times 10^8$ injected particles), and no apparent damage was observed in this group. An example histology slide is presented in Figure 10. This suggested that a sufficient concentration of PSNEs should be administered so that there will be enough IC activity to create the desired bioeffect (*i.e.,* ischemic or hemorrhagic lesion). In all, we can see from these two groups that in order to consistently create lesions in the brain, a relatively high concentration of PSNEs should be administered and the ultrasound pressure should exceed the PSNE-nucleated IC threshold.

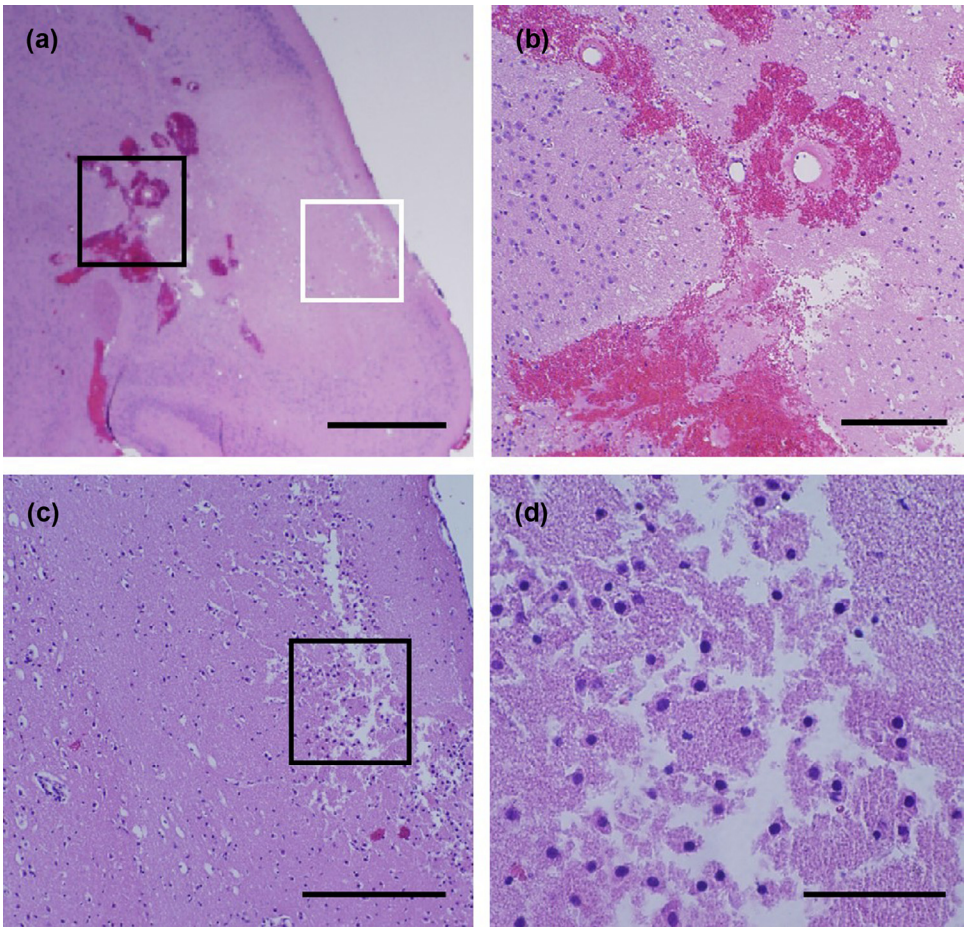

Fig. 6. Histologic appearance of a lesion 24 h after sonication. (a) Brain tissue necrosis with a loss of tissue structure. (b) High magnification view of the area outlined in black in (a). Extensive hemorrhages occurred at one side of the lesion where large vessels were abundant and were ruptured by the IC. The red blood cells were obvious around the damaged vessel. (c) High-magnification view of the area outlined in white box in (a). Dead neurons with shrunken nuclei and empty cytoplasms were abundant within the lesion. (d) High-magnification view of the area outlined in black in (c). Some tissues close to the edge of the brain appeared spongy and semiliquid, suggesting mechanical destruction. Scale bars are 1 mm in (a), 0.2 mm in (b) & (c) and 0.05 mm in (d). IC = inertial cavitation.

DISCUSSION

In this pilot study, we tested two central hypotheses: (i) circulating PFB-based PSNEs could be vaporized in the brain blood vessels with sub-MHz transcranial FUS tone bursts below 2 MPa, and (ii) focal mechanical ablation of brain tissue was possible with PFB-based PSNEs combined with sub-MHz FUS. To test the first hypothesis, a 740-kHz FUS transducer transmitted 15-ms tone bursts into the mouse brain through the skull after IV injection of PFB-based PSNEs. A PCD sensitive to the f/2 subharmonic of the FUS transducer monitored for IC nucleated by vaporized PSNEs. A significant increase in average power for the processed PCD signals was observed once the FUS transmitted a PNP that exceeded 1.2 MPa, suggesting successful vaporization of circulating PFB-based PSNEs. This "apparent" threshold for IC activity in the brain that sonicated at 740 kHz compared favorably with a recent study in which PFB-based PSNEs were vaporized in brain blood vessels with 6.7-ms tone bursts at 1.5-MHz (Wu et al. 2018). In the documented study, significant IC activity was detected *via* PCD when the transmitted derated PNP was at least 0.9 MPa (Wu et al. 2018). The non-derated PNP based on 18.1% loss due to skull attenuation at 1.5 MHz (Choi et al. 2007) is approximately 1.125 MPa, which is comparable with our non-derated pressure for initiating IC activity at 740 kHz. Importantly, the estimated time-average acoustic power for pulses exceeding the ''apparent'' IC threshold ranged from 0.11−0.24 W. We do not anticipate significant heating in the skull leading to thermal damage at the periphery of the brain at these power levels based on our unpublished studies,

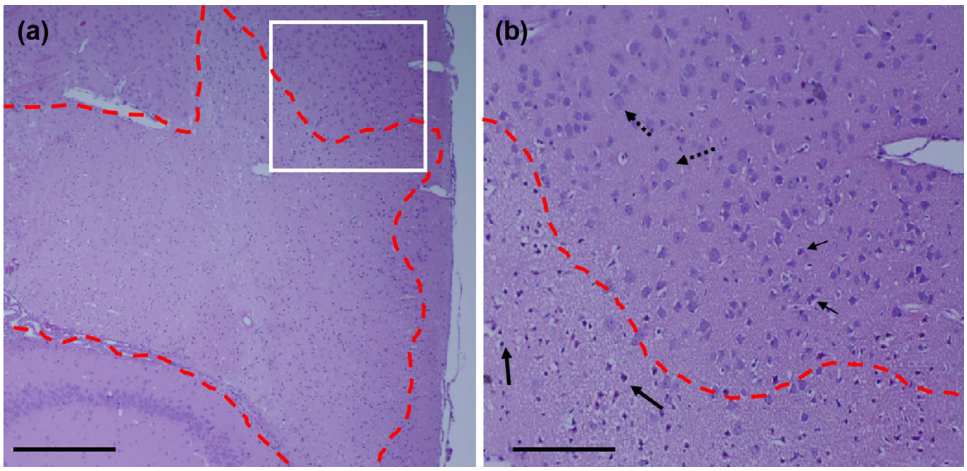

Fig. 7. Histologic example of ischemic lesions with sharp boundaries from high pressure and high PSNE concentration group. (a) A lesion was formed at the targeted area that has a well-defined boundary (red dash lines) of living and dead cells. (b) Dead neurons with shrunken nuclei and empty cytoplasms (solid arrows) were formed within the circumference of the lesion (red dash lines). Living cells (dotted arrows) were abundant outside of the lesion. There is a transition zone with some cells with pyknotic nuclei (small arrows). Scale bar is 1 mm in (a) and 0.1 mm in (b). PSNE = phase-shift nanoemulsions.

and thus we explored these pressures for focal nonthermal ablation of brain tissue.

Reportedly, the mean circulation half-life for PFB-based PSNEs is approximately 10 min, which is about three times the mean half-life for encapsulated MBs (Sheeran et al. 2015). Thus, a single bolus PSNE injection may serve as IC nuclei for several min. Our results displayed in Figure 4a, which show significant enhancement

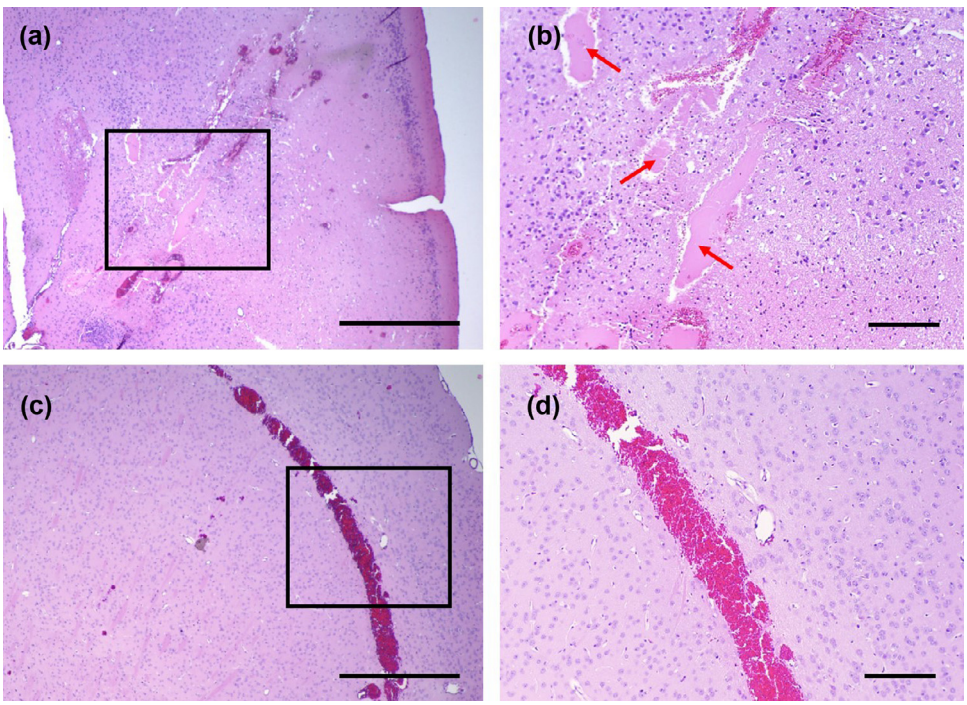

Fig. 8. Histologic example of damages appeared less frequently in high pressure and high PSNE concentration group. (a) An empty cavity was created within the lesion (1 out of 4 mice), and the proteinaceous fluid filled into the cavity. (b) High resolution view of the area in the black box in (a). Proteinaceous fluid is pointed with a red arrow. (c) Extensive red blood cell extravasation at the tissue boundary, which indicated a strong boundary effect due to the tissue boundary. (d) High-resolution view of the area in the black box in (c). Scale bars are 1 mm in (a) & (c) and 0.2 mm in (b) & (d). PSNE = phase-shift nanoemulsions.

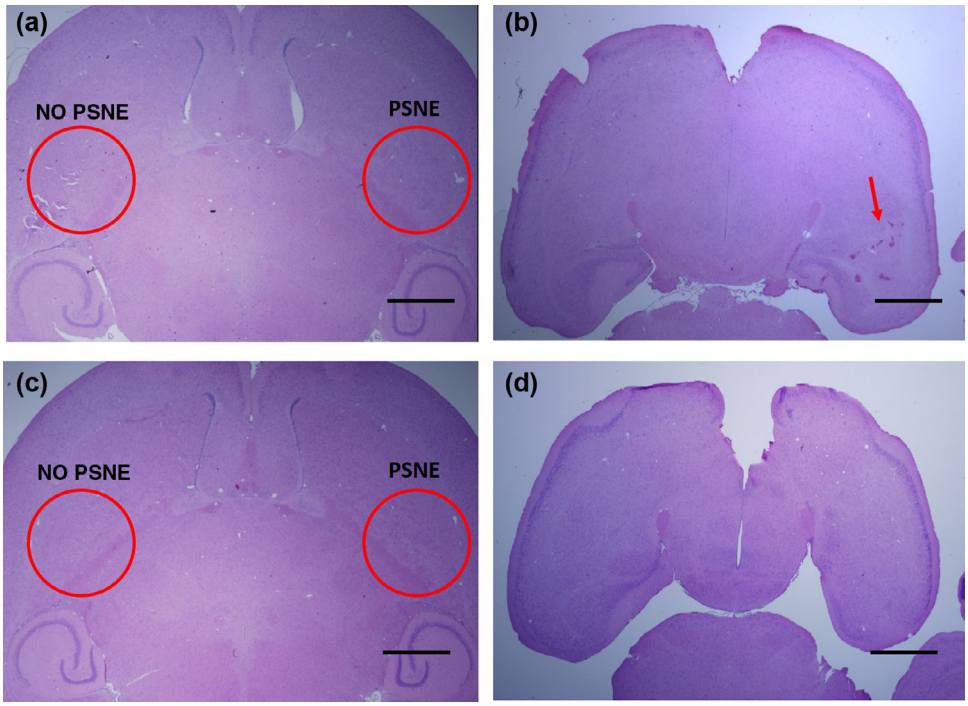

Fig. 9. Examples of H&E staining from two mice that were injected with non-diluted PSNEs and sonicated at 1.5 MPa. (a) The slice that was located 3 mm from the bottom of the brain of subject 1. No apparent damage was created by sonication within the targeted area with or without PSNEs. (b) H&E slice from the bottom of the brain from subject 1. Red arrow is pointing at the side that was sonicated with PSNEs. Some micro-hemorrhage was observed, but it was not as extensive as mice sonicated at a higher pressure. This was observed only in 1 of the 4 mice. (c) H&E slice that was located 3 mm from the bottom of the brain of subject 2. No apparent damage was found in both side. (d) H&E slice from the bottom of the brain of subject 2. There was no apparent damage at the bottom in both side. Scale bars are 1 mm. H&E = hematoxylin and eosin; PSNE = phase-shift nanoemulsions.

in acoustic emissions for 10 min post-injection of the nanoemulsions, support this idea. Additional bolus injections of PSNEs could be administered to maintain an ideal concentration of IC nuclei for longer than 10 min if needed.

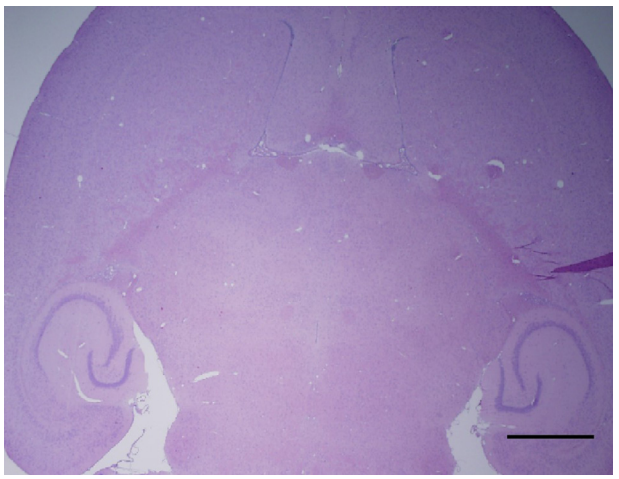

Fig. 10. H&E staining example of mice that were injected with 5 times diluted PSNEs and were exposed with high ultrasound pressure (1.8 MPa). No apparent damage was found on either side, with or without PSNEs. Scale bar is 1 mm. H&E = hematoxylin and eosin; PSNE = phase-shift nanoemulsions.

Next, we used histology to analyze the impact of sustained localized IC activity on the brain tissue and blood vessels. We identified contiguous regions of dead tissue (lesions) in all cases where significant IC activity was detected. The lesions appeared to have a sharp boundary between living and dead cells, and the lesions' size and shape were comparable to the FWHM acoustic pressure contour of the beam plot at the focus of the transducer. In addition, there was less or no damage in the pre-focal region, which was commonly found when other exogenous agents were used to nucleate cavitation (McDannold et al. 2016; Moyer et al. 2015; Phillips et al. 2013). These findings indicate that we could utilize this technique to create a confined lesion at acoustic focus. Comparatively, more severe damage could be found at the post focal region close to the skull base, which presumably was due to reflection at the skull wall. Reflections from the skull were expected given the long focus (FWHM: 12 mm) of the transducer relative to the thickness of the mouse brain (6 mm) in this study. A future study using a larger animal or a transducer with a shorter focus would mitigate this problem.

We speculated that cavitation-induced vascular disruption and ischemia would be the predominant mechanism for lesion formation in this technique. Intravascular PSNE vaporization and IC can create shock waves and/or high-velocity jets that could damage blood vessels. Cumulative vascular damage may severely disrupt perfusion locally, leading to focal ischemia in the brain. This was supported by observation of microhemorrhage, which was the typical capillary damage reported in bubble-enhanced ablation (McDannold et al. 2006). Lesions were not detected in brain regions where FUS exposures were not above 1.2 MPa or in mice that were injected with PSNEs at low concentration (*i.e.,* five times diluted). In both cases, acoustic emissions were negligible, which suggests that PSNE-nucleated IC activity was minimal. It is worth noting that the H&E staining of some mice contained some areas without evidence of ruptured blood vessels or erythrocyte extravasation but still had ischemic lesions (Fig. 6c, 6d). This is presumably due to the generation of occlusion or constriction of the blood vessels. It has been reported previously that HIFU in combination with ultrasound contrast agents (PSNEs or MBs) can occlude blood vessels (Al-Mahrouki et al. 2014; Hwang et al. 2005; Hynynen et al. 1996; Kripfgans et al. 2005; Zhang et al. 2010). Spasms in blood vessels also have been reported in previous work (Raymond et al. 2007). There are several mechanisms through which cavitation may suppress perfusion, resulting in ischemia. The intensity and/or duration of cavitation activity may dictate the mechanism of vascular shutdown. As such, it will be essential to control the level of vasculature damage with a feedback system, which could be achieved by an acoustic detection system (O'Reilly and Hynynen 2012; Sun et al. 2017).

There were a few limitations in this pilot study. While we successfully created brain lesions, there were some cases that severe damage and tissue homogenization occurred at the base of the brain, which presumably was caused by reflection. Therefore, use of a larger animal model most likely would resolve this limitation. In addition to that, we did not perform a longitudinal study and therefore lack information regarding the timing for formation of the brain lesions or their impact on the health and survival of the animal. However, the findings of the study do provide valuable information on the parameters that may be utilized for focal ablation of brain tumors in a larger animal model.

CONCLUSIONS

In this study, we successfully vaporized PSNEs to facilitate the transcranial HIFU mechanical ablation in the brain. The results suggested that PSNEs can significantly reduce the time-average power and pressure compared with traditional HIFU thermal ablation. The damage created by PSNE-facilitated ablation is consistent with previous bubble-facilitated ablation, including localized vasculature damage, ischemic strokes and tissue fragmentation. We are therefore encouraged to further investigate whether we are able to ablate a tumor in a glioblastoma model in the future. We foresee that the success of our study could improve the efficacy and efficiency of HIFU ablation and expand the treatment envelope, which would benefit more patients.

Acknowledgments—This work was supported by NIH grants (P01 CA17464501 and a Boston University and Brigham and Women's Hospital training grant BU-BWH partnership.

REFERENCES

Al-Mahrouki AA, Iradji S, Tran WT, Czarnota GJ. Cellular characterization of ultrasound-stimulated microbubble radiation enhancement in a prostate cancer xenograft model. Dis Model Mech 2014;7:363–372.

Arvanitis CD, Vykhodtseva N, Jolesz F, Livingstone M, McDannold N. Cavitation-enhanced nonthermal ablation in deep brain targets: Feasibility in a large animal model. J Neurosurg 2016;124:1450–1459.

Azuma T, Kawabata K, Umemura S, Ogihara M, Kubota J, Sasaki A, Furuhata H. Bubble generation by standing wave in water surrounded by cranium with transcranial ultrasonic beam. Jpn J Appl Phys 2005;44:4625–4630.

Baron C, Aubry J-F, Tanter M, Meairs S, Fink M. Simulation of intracranial acoustic fields in clinical trials of sonothrombolysis. Ultrasound Med Biol 2009;35:1148–1158.

Burke CW, Klibanov AL, Sheehan JP, Price RJ. Inhibition of glioma growth by microbubble activation in a subcutaneous model using low duty cycle ultrasound without significant heating: Laboratory investigation. J Neurosurg 2011;114:1654–1661.

Chaichana KL, Cabrera-Aldana EE, Jusue-Torres I, Wijesekera O, Olivi A, Rahman M, Quinones-Hinojosa A. When gross total resection of a glioblastoma is possible, how much resection should be achieved? World Neurosurg 2014;82:e257–e265.

Chaichana KL, Jusue-Torres I, Navarro-Ramirez R, Raza SM, Pascual-Gallego M, Ibrahim A, Hernandez-Hermann M, Gomez L, Ye X, Weingart JD, Olivi A, Blakeley J, Gallia GL, Lim M, Brem H, Quinones-Hinojosa A. Establishing percent resection and residual volume thresholds affecting survival and recurrence for patients with newly diagnosed intracranial glioblastoma. Neuro Oncol 2014;16:113–122.

Charrois GJ, Allen TM. Rate of biodistribution of STEALTH liposomes to tumor and skin: Influence of liposome diameter and implications for toxicity and therapeutic activity. Biochim Biophys Acta 2003;1609:102–108.

Choi JJ, Pernot M, Small SA, Konofagou EE. Noninvasive, transcranial and localized opening of the blood-brain barrier using focused ultrasound in mice. Ultrasound Med Biol 2007;33:95–104.

Clement GT, Sun J, Giesecke T, Hynynen K. A hemisphere array for non-invasive ultrasound brain therapy and surgery. Phys Med Biol 2000;45:3707–3719.

Coluccia D, Fandino J, Schwyzer L, O'Gorman R, Remonda L, Anon J, Martin E, Werner B. First noninvasive thermal ablation of a brain tumor with MR-guided focused ultrasound. J Ther Ultrasound 2014;2:17.

Czarnota GJ, Karshafian R, Burns PN, Wong S, Al Mahrouki A, Lee JW, Caissie A, Tran W, Kim C, Furukawa M, Wong E, Giles A. Tumor radiation response enhancement by acoustical stimulation of the vasculature. Proc Natl Acad Sci U S A 2012;109:E2033–E2041.

De la Garza-Ramos R, Kerezoudis P, Tamargo RJ, Brem H, Huang J, Bydon M. Surgical complications following malignant brain tumor surgery: An analysis of 2002–2011 data. Clin Neurol Neurosurg 2016;140:6–10.

Elias WJ, Lipsman N, Ondo WG, Ghanouni P, Kim YG, Lee W, Schwartz M, Hynynen K, Lozano AM, Shah BB, Huss D, Dallapiazza RF, Gwinn R, Witt J, Ro S, Eisenberg HM, Fishman PS, Gandhi D, Halpern CH, Chuang R, Butts Pauly K, Tierney TS, Hayes MT, Cosgrove GR, Yamaguchi T, Abe K, Taira T, Chang JW. A randomized trial of focused ultrasound thalamotomy for essential tremor. N Engl J Med 2016;375:730–739.

Fabiilli ML, Haworth KJ, Sebastian IE, Kripfgans OD, Carson PL, Fowlkes JB. Delivery of chlorambucil using an acoustically-triggered perfluoropentane emulsion. Ultrasound Med Biol 2010;36:1364–1375.

Gianfelice D, Gupta C, Kucharczyk W, Bret P, Havill D, Clemons M. Palliative treatment of painful bone metastases with MR imaging–guided focused ultrasound. Radiology 2008;249:355–363.

Giesecke T, Hynynen K. Ultrasound-mediated cavitation thresholds of liquid perfluorocarbon droplets in vitro. Ultrasound Med Biol 2003;29:1359–1365.

Huang Y, Vykhodtseva NI, Hynynen K. Creating brain lesions with low-intensity focused ultrasound with microbubbles: A rat study at half a megahertz. Ultrasound Med Biol 2013;39:1420–1428.

Huss DS, Dallapiazza RF, Shah BB, Harrison MB, Diamond J, Elias WJ. Functional assessment and quality of life in essential tremor with bilateral or unilateral DBS and focused ultrasound thalamotomy: Functional assessment of ET treated by DBS or FUS. Mov Disord 2015;30:1937–1943.

Hwang JH, Brayman AA, Reidy MA, Matula TJ, Kimmey MB, Crum LA. Vascular effects induced by combined 1-MHz ultrasound and microbubble contrast agent treatments in vivo. Ultrasound Med Biol 2005;31:553–564.

Hynynen K. The threshold for thermally significant cavitation in dog's thigh muscle in vivo. Ultrasound Med Biol 1991;17:157–169.

Hynynen K, Colucci V, Chung A, Jolesz F. Noninvasive arterial occlusion using MRI-guided focused ultrasound. Ultrasound Med Biol 1996;22:1071–1077.

Ishida O, Maruyama K, Sasaki K, Iwatsuru M. Size-dependent extravasation and interstitial localization of polyethyleneglycol liposomes in solid tumor-bearing mice. Int J Pharm 1999;190:49–56.

Song Junho, Pulkkinen A, Huang Yuexi, Hynynen K. Investigation of standing-wave formation in a human skull for a clinical prototype of a large-aperture, transcranial MR-guided focused ultrasound (MRgFUS) phased array: An experimental and simulation study. IEEE Trans Biomed Eng 2012;59:435–444.

Karsy M, Yoon N, Boettcher L, Jensen R, Shah L, MacDonald J, Menacho ST. Surgical treatment of glioblastoma in the elderly: The impact of complications. J Neurooncol 2018;138:123–132.

Khokhlova TD, Wang Y-N, Simon JC, Cunitz BW, Starr F, Paun M, Crum LA, Bailey MR, Khokhlova VA. Ultrasound-guided tissue fractionation by high intensity focused ultrasound in an in vivo porcine liver model. Proc Natl Acad Sci U S A 2014;111:8161–8166.

Khokhlova VA, Fowlkes JB, Roberts WW, Schade GR, Xu Z, Khokhlova TD, Hall TL, Maxwell AD, Wang Y-N, Cain CA. Histotripsy methods in mechanical disintegration of tissue: Towards clinical applications. Int J Hyperthermia 2015;31:145–162.

Koch MO, Gardner T, Cheng L, Fedewa RJ, Seip R, Sanghvi NT. Phase I/II trial of high intensity focused ultrasound for the treatment of previously untreated localized prostate cancer. J Urol 2007;178:2366–2371.

Kopechek JA, Park E-J, Zhang Y-Z, Vykhodtseva NI, McDannold NJ, Porter TM. Cavitation-enhanced MR-guided focused ultrasound ablation of rabbit tumors in vivo using phase shift nanoemulsions. Phys Med Biol 2014;59:3465–3481.

Kripfgans OD, Orifici CM, Carson PL, Ives KA, Eldevik OP, Fowlkes JB. Acoustic droplet vaporization for temporal and spatial control of tissue occlusion: A kidney study. IEEE Trans Ultrason Ferroelectr Freq Control 2005;52:1101–1110.

Maeda H, Wu J, Sawa T, Matsumura Y, Hori K. Tumor vascular permeability and the EPR effect in macromolecular therapeutics: A review. J Control Release 2000;65:271–284.

Maxwell AD, Wang T-Y, Cain CA, Fowlkes JB, Sapozhnikov OA, Bailey MR, Xu Z. Cavitation clouds created by shock scattering from bubbles during histotripsy. J Acoust Soc Am 2011;130:1888–1898.

McDannold NJ, Vykhodtseva NI, Hynynen K. Microbubble contrast agent with focused ultrasound to create brain lesions at low power levels: MR imaging and histologic study in rabbits. Radiology 2006;241:95–106.

McDannold N, Clement GT, Black P, Jolesz F, Hynynen K. Transcranial magnetic resonance imaging–guided focused ultrasound surgery of brain tumors. Neurosurgery 2010;66:323–332.

McDannold N, Zhang Y-Z, Power C, Jolesz F, Vykhodtseva N. Nonthermal ablation with microbubble-enhanced focused ultrasound close to the optic tract without affecting nerve function: Laboratory investigation. J Neurosurg 2013;119:1208–1220.

McDannold N, Zhang Y, Vykhodtseva N. Nonthermal ablation in the rat brain using focused ultrasound and an ultrasound contrast agent: Long-term effects. J Neurosurg 2016;125:1539–1548.

Moyer LC, Timbie KF, Sheeran PS, Price RJ, Miller GW, Dayton PA. High-intensity focused ultrasound ablation enhancement in vivo via phase-shift nanodroplets compared to microbubbles. J Ther Ultrasound 2015;3:7. doi: 10.1186/s40349-015-0029-4. Accessed July 15, 2018.

Nomura T, Koreeda N, Yamashita F, Takakura Y, Hashida M. Effect of particle size and charge on the disposition of lipid carriers after intratumoral injection into tissue-isolated tumors. Pharm Res 1998;15:128–132.

O'Reilly MA, Hynynen K. Blood-brain barrier: Real-time feedback-controlled focused ultrasound disruption by using an acoustic emissions–based controller. Radiology 2012;263:96–106.

Paxinos G, Franklin KBJ. The mouse brain in stereotaxic coordinates. Houston: Gulf Professional Publishing; 2004.

Phillips LC, Puett C, Sheeran PS, Dayton PA, Wilson Miller G, Matsunaga TO. Phase-shift perfluorocarbon agents enhance high intensity focused ultrasound thermal delivery with reduced near-field heating. J Acoust Soc Am 2013;134:1473–1482.

Raymond SB, Skoch J, Hynynen K, Bacskai BJ. Multiphoton imaging of ultrasound/optison mediated cerebrovascular effects *in vivo*. J Cereb Blood Flow Metab 2007;27:393–403.

Roberts WW, Hall TL, Ives K, Wolf JS, Fowlkes JB, Cain CA. Pulsed cavitational ultrasound: A noninvasive technology for controlled tissue ablation (histotripsy) in the rabbit kidney. J Urol 2006;175:734–738.

Schad KC, Hynynen K. In vitro characterization of perfluorocarbon droplets for focused ultrasound therapy. Phys Med Biol 2010;55:4933–4947.

Sheeran PS, Luois S, Dayton PA, Matsunaga TO. Formulation and acoustic studies of a new phase-shift agent for diagnostic and therapeutic ultrasound. Langmuir 2011;27:10412–10420.

Sheeran PS, Luois SH, Mullin LB, Matsunaga TO, Dayton PA. Design of ultrasonically-activatable nanoparticles using low boiling point perfluorocarbons. Biomaterials 2012;33:3262–3269.

Sheeran PS, Matsunaga TO, Dayton PA. Phase-transition thresholds and vaporization phenomena for ultrasound phase-change nanoemulsions assessed via high-speed optical microscopy. Phys Med Biol 2013;58:4513–4534.

Sheeran PS, Rojas JD, Puett C, Hjelmquist J, Arena CB, Dayton PA. Contrast-enhanced ultrasound imaging and in vivo circulatory kinetics with low-boiling-point nanoscale phase-change perfluorocarbon agents. Ultrasound Med Biol 2015;41:814–831.

Stewart EA, Rabinovici J, Tempany CMC, Inbar Y, Regan L, Gastout B, Hesley G, Kim HS, Hengst S, Gedroye WM. Clinical outcomes of focused ultrasound surgery for the treatment of uterine fibroids. Fertil Steril 2006;85:22–29.

Suk JS, Xu Q, Kim N, Hanes J, Ensign LM. PEGylation as a strategy for improving nanoparticle-based drug and gene delivery. Adv Drug Deliv Rev 2016;99:28–51.

Sun T, Zhang Y, Power C, Alexander PM, Sutton JT, Aryal M, Vykhodtseva N, Miller EL, McDannold NJ. Closed-loop control of targeted ultrasound drug delivery across the blood–brain/tumor barriers in a rat glioma model. Proc Natl Acad Sci U S A 2017;114:E10281–E10290.

Vlaisavljevich E, Lin K-W, Maxwell A, Warnez MT, Mancia L, Singh R, Putnam AJ, Fowlkes B, Johnsen E, Cain C, Xu Z. Effects of

ultrasound frequency and tissue stiffness on the histotripsy intrinsic threshold for cavitation. Ultrasound Med Biol 2015;41:1651–1667.
Wang Y-N, Khokhlova T, Bailey M, Hwang JH, Khokhlova V. Histological and biochemical analysis of mechanical and thermal bioeffects in boiling histotripsy lesions induced by high intensity focused ultrasound. Ultrasound Med Biol 2013;39:424–438.
Wang Z, Moehring MA, Voie AH, Furuhata H. In vitro evaluation of dual mode ultrasonic thrombolysis method for transcranial application with an occlusive thrombosis model. Ultrasound Med Biol 2008;34:96–102.
Weller M, van den Bent M, Hopkins K, Tonn JC, Stupp R, Falini A, Cohen-Jonathan-Moyal E, Frappaz D, Henriksson R, Balana C, Chinot O, Ram Z, Reifenberger G, Soffietti R, Wick W. EANO guideline for the diagnosis and treatment of anaplastic gliomas and glioblastoma. Lancet Oncol 2014;15:e395–e403.
White PJ, Clement GT, Hynynen K. Longitudinal and shear mode ultrasound propagation in human skull bone. Ultrasound Med Biol 2006;32:1085–1096.
Wu S-K, Chu P-C, Chai W-Y, Kang S-T, Tsai C-H, Fan C-H, Yeh C-K, Liu H-L. Characterization of different microbubbles in assisting focused ultrasound-induced blood-brain barrier opening. Sci Rep 2017;7:46689.
Wu S-Y, Fix SM, Arena CB, Chen CC, Zheng W, Olumolade OO, Papadopoulou V, Novell A, Dayton PA, Konofagou EE. Focused ultrasound-facilitated brain drug delivery using optimized nanodroplets: Vaporization efficiency dictates large molecular delivery. Phys Med Biol 2018;63 035002.
Xu Z, Fowlkes JB, Rothman ED, Levin AM, Cain CA. Controlled ultrasound tissue erosion: The role of dynamic interaction between insonation and microbubble activity. J Acoust Soc Am 2005;117:424–435.
Yuan F, Dellian M, Fukumura D, Leunig M, Berk DA, Torchilin VP, Jain RK. Vascular permeability in a human tumor xenograft: Molecular size dependence and cutoff size. Cancer Res 1995;55:3752–3756.
Zhang M, Fabiilli ML, Haworth KJ, Fowlkes JB, Kripfgans OD, Roberts WW, Ives KA, Carson PL. Initial investigation of acoustic droplet vaporization for occlusion in canine kidney. Ultrasound Med Biol 2010;36:1691–1703.
Zhang P, Kopechek JA, Porter TM. The impact of vaporized nanoemulsions on ultrasound-mediated ablation. J Ther Ultrasound 2013;1:2.
Zhang P, Porter T. An in vitro study of a phase-shift nanoemulsion: A potential nucleation agent for bubble-enhanced HIFU tumor ablation. Ultrasound Med Biol 2010;36:1856–1866.
Zhang X, Owens GE, Gurm HS, Ding Y, Cain CA. Noninvasive thrombolysis using histotripsy beyond the Intrinsic threshold (microtripsy). IEEE Trans Ultrason Ferroelectr Freq Control 2015;62:1342–1355.